

*Article*

## Intelligent Backstepping System to Increase Input Shaping Performance in Suppressing Residual Vibration of a Flexible-Joint Robot Manipulator

Withit Chatlatanagulchai<sup>a</sup>, Sirichai Nithi-uthai<sup>b</sup>, and Pisit Intarawirat<sup>c</sup>

Control of Robot and Vibration Laboratory, Department of Mechanical Engineering, Faculty of Engineering, Kasetsart University, 50 Ngam Wong Wan Rd, Lat Yao, Chatuchak, Bangkok 10900, Thailand  
E-mail: <sup>a</sup>fengwtc@ku.ac.th (Corresponding author), <sup>b</sup>timberwolf\_777@hotmail.com, <sup>c</sup>pisit.intarawirat@gmail.com

**Abstract.** Input shaping technique can be used to suppress residual vibration, occurring from moving rapidly a flexible system from one point to another point. An input shaping filter produces a shaped input signal that avoids exciting the flexible modes of the flexible system. The technique requires accurate knowledge of mode parameters. When the plant model is not accurate, performance of the input shaper degrades. Several robust input shapers were proposed to handle this inaccuracy at the expense of longer move time. The purpose of this paper is, for the first time, to present an application of an intelligent backstepping system to matching of the resulting closed-loop system with a reference model. The input shaper can then be designed from the mode parameters of the reference model. Because the reference model is accurate even when the plant model is not, the input shaper needs not be robust, resulting in shorter move time. The intelligent backstepping system consists of a three-layer neural network, a variable structure controller, and a backstepping controller. The neural network is used as a black-box model in case when the plant model is unknown, making the proposed system model-independent. The adaptive property of the neural network also makes the proposed system suitable for nonlinear, time-varying, or configuration-dependent systems. The variable structure controller handles the uncertainty arisen in the system. The backstepping controller, through its virtual controls, provides a means for the control authority to reach the unmatched uncertainty in the system. This study contains simulation and experimental results on a flexible-joint robot manipulator. The results showed that this proposed intelligent input shaping system outperformed previously proposed robust input shapers in terms of allowable uncertainty amount and move time. The proposed system is also relatively easy to apply because it does not require the plant model.

**Keywords:** Input shaping, vibration reduction, backstepping, neural network, variable structure control, flexible joint.

ENGINEERING JOURNAL Volume 21 Issue 5

Received 11 July 2016

Accepted 21 March 2017

Published 29 September 2017

Online at <http://www.engj.org/>

DOI:10.4186/ej.2017.21.5.203

**Nomenclature:**

$\varepsilon$	perturbed parameter
$\varepsilon_i$	approximation error
$\theta_1$	absolute link angular position
$\theta_2$	absolute motor angular position
$\omega_a$	actual natural frequency
$\omega_d$	damped natural frequency
$\omega_{ni}$	natural frequency of the $i^{th}$ mode
$\zeta$	damping ratio
$A_i$	impulse amplitudes
BMM-IS	backstepping model matching with input shaping
$d_{ai}$	disturbance at the $i^{th}$ subsystem
$d_{aiU}$	upper bound of the disturbance
$e$	model output tracking error
$EI$	extra-insensitive
$g(\cdot)$	a nonlinear function to be approximated
$k_{slin}$	linearized spring constant
$l$	number of hidden-layer nodes
PEI-ISs	perturbation-based extra-insensitive input shapers
$r_b$	original reference input
$r_s$	shaped reference input
$s(\cdot)$	activation function such as sigmoid function
$t_i$	time locations of the impulses
$T_1$	torque produced by the motor coil
$T_2$	torque output from deadzone
$T_3$	torque output from backlash
$T_d$	damped period
$u$	control input
$u_c$	controller output
$v$	motor input voltage
$V$	percentage vibration

$V^*$	ideal weight matrix
$V_{iU}$	upper bound of the ideal weight matrix
$\hat{V}$	estimate of the ideal weight matrix
$\tilde{V}$	weight estimation error
$V_{lim}$	percentage vibration limit
$W^*$	ideal weight matrix
$W_{iU}$	upper bound of the ideal weight matrix
$\hat{W}$	estimate of the ideal weight matrix
$\tilde{W}$	weight estimation error
$y$	plant output
$y_m$	reference model output
$z_i$	inputs to the neural network
ZV	zero vibration input shaper
ZVD	zero vibration and derivative input shaper

## 1. Introduction

Input shaping is a technique to reduce residual vibration. The technique is based on destructive interference of impulse responses, that is, an impulse response can be cancelled by another impulse response, given appropriate impulse amplitudes and applied times. The input shaping was originally proposed under the name Posicast control by Smith in [1]; Smith in [2]; and Tallman and Smith in [3]. The first application of the Posicast control to robot transport of suspended objects was performed by Starr in [4] and Starr in [5], whose method was further generalized by Strip in [6]. Singer and Seering in [7] extended the Posicast control by increasing its robustness to parameter uncertainty and patented the technique under the name input shaping.

Applications of the input shaping technique range from gantry crane (Sorensen *et al.* in [8]), bridge crane (Peng *et al.* in [9]), tower crane (Huey *et al.* in [10]), boom crane (Huang *et al.* in [11]), flexible-link robot (Chatlatanagulchai *et al.* in [12]), flexible-joint robot (Chatlatanagulchai and Saeheng in [13]), liquid sloshing in container (Baozeng and Lemei in [14]), flexible spacecraft (Zhang and Zhang in [15]), coordinate measuring machine (Singhose *et al.* in [16]), cam follower (Pridgen and Singhose in [17]), telescopic handler (Park and Chang in [18]), cherry picker (Hongxia *et al.* in [19]), dual solenoid actuator (Yu and Chang in [20]), MEMS contact switch (Do *et al.* in [21]), hard disk drive (La-orpacharapan and Pao in [22]), cable-driven crane (Huey and Singhose in [23]), high-rise elevator (Fortgang *et al.* in [24]), wave suppression (Yang and Liang in [25]), atomic force microscopy (Schitter *et al.* in [26]), CNC machine tool (Altintas and Khoshdarregi in [27]), micro-milling machine (Fortgang and Singhose in [28]), wafer stage in chip manufacturing (Roover and Sperling in [29]), automated highway (Bae and Gerdes in [30]), brushless motor (Chang *et al.* in [31]), cooperative motion between two robots (Zhang *et al.* in [32]), twin rotor (Toha and Tokhi in [33]), quadrotor with sling load (Palunko *et al.* in [34]), helicopter with sling load (Potter *et al.* in [35]), nuclear power plant's fuel transport system (Shah and Hong in [36]), to automotive wiper (Ahmad *et al.* in [37]).

A disadvantage of using the input shaping technique is that the input shaper extends the duration of the shaped reference input by the length of the shaper, which is equal to the time location of the last impulse subtracted by that of the first impulse. Since the design parameters of the input shaper are obtained from the mode parameters, the vibration suppression performance of the input shaper also depends largely on the accuracy of the modelled mode parameters. Because the plant model can never represent the actual system perfectly, several robust input shapers have been proposed in the literature to maintain good vibration suppression performance in the presence of uncertainty in the plant model. Singer and Seering in [7] proposed the so-called ZVD<sup>k</sup> input shaper by including higher-order derivatives of the zero residual vibration expression as additional constraints to solve for the input shaper. Singhose *et al.* in [38] presented the so-called extra-insensitive (EI) shaper. This shaper is designed from relaxing the requirement that the residual vibration must be zero when the system model is exactly known. By allowing a low level of vibration, the robustness of the input shaper can be increased significantly. Singer and Seering in [39] proposed a so-called frequency sampling method to establish constraints on the vibration amplitude over a specified range of frequencies. Because the insensitivity to frequency variation can be specified by the designer, the resulting shaper is called specified-insensitivity (SI) shaper. Rew *et al.* in [40] proposed perturbation-based extra-insensitive input shapers (PEI-ISs). The PEI-ISs are multiplication of a series of ZV input shapers in the Laplace domain. The series includes ZV input shapers whose impulse times are slightly perturbed. PEI-ISs are simple and were shown to be more robust to parameter variation than the EI shaper. They were also shown to have less transient vibration than the EI and SI shapers. However, the SI shaper has shorter duration than the PEI-ISs. Singh in [41] proposed a robust input shaper called minimax input shaper. The minimax input shaper aims to move the system from rest to rest while minimizes the maximum magnitude of the residual states over a range of uncertain parameter values. Pao *et al.* in [42] developed an input shaping design approach that took into account the knowledge of the probability distribution of the system natural frequency about its modeled value. The proposed input shaper has the ability to deal with the statistical nature of plant parameter variations. Singh *et al.* in [43] presented an improvement over the shaper of Pao *et al.* in [42], which may become computationally expensive when the dimension of the parameters grows. The approximate of the stochastic system state by using finite-dimensional series expansion in the stochastic space was applied. Magee and Book in [44] presented a modified command filtering technique in discrete time. This modified filter ensures a more uniform output for each discrete-time sample as the system parameters vary with time. Conord and Singh in [45] formulated the design of the robust input shaper as an optimization problem having linear matrix

inequalities (LMI) constraints. Vaughan *et al.* in [46] and [47] compared among several types of robust input shapers and also investigated combining the specified negative amplitude (SNA) shaper (Singhose *et al.* in [48]) with the SI shaper.

The previously proposed robust input shapers have more robustness to the mode parameter uncertainty at the price of having more impulses in the input shaper sequence, hence slower time to reach final reference value. Moreover, they require plant model either to use in their algorithms or to obtain the modelled mode parameters.

Advantages of the proposed technique, over the previously proposed robust input shaping techniques, are as follows:

- Substantially larger amount of uncertainty in the mode parameters can be tolerated.
- Shaped reference input has short duration, and its duration does not increase with the amount of insensitivity, as in the case of the robust input shaping.
- The proposed system applies to nonlinear, time-varying, or configuration-dependent plant.
- The proposed system is model-independent, that is, the accurate knowledge of the plant model is not required in designing the system.

In this paper, an intelligent backstepping input shaping (IBS-IS) technique is proposed. Three-layer neural networks are used to represent the unknown plant as in black-box system identification. The system uses the backstepping and variable structure controllers as feedback controllers in matching the resulting closed-loop system to a reference model. The backstepping structure provides a means for the control authority to reach the unmatched uncertainty in the system. The variable structure controller handles the uncertainty. The ZV input shaper is placed outside of the closed-loop system and is designed from accurate mode parameters of the reference model. Simulation and experiment on a flexible-joint robot manipulator confirm the advantages of the proposed technique.

## 2. Materials and Methods

### 2.1. Input Shaping

Figure 1 shows input shaping for a flexible system.  $\bar{r}$  is the original reference input, normally a step signal. The switch is for the user to select whether to use the input shaper or not. The input shaper is a cascade of FIR filters; each filter handles one vibratory mode. The design parameters of the input shaper are the impulse amplitudes  $\bar{F}_i$  and the time locations of the impulses  $t_i$ . The shaped reference input  $r$ , which is the output of the input shaper, is given to the flexible system to follow. The flexible system can be open-loop or closed-loop with known natural frequencies and damping ratios.  $\omega_{ni}$  are the natural frequency of the  $i^{\text{th}}$  mode whereas  $\zeta$  is the damping ratio; they are so-called mode parameters. The parameters  $\bar{F}_i$  and  $t_i$  are designed such that the shaped reference input  $r$  avoids exciting the flexible modes, resulting in no residual vibration in the output  $y$ .

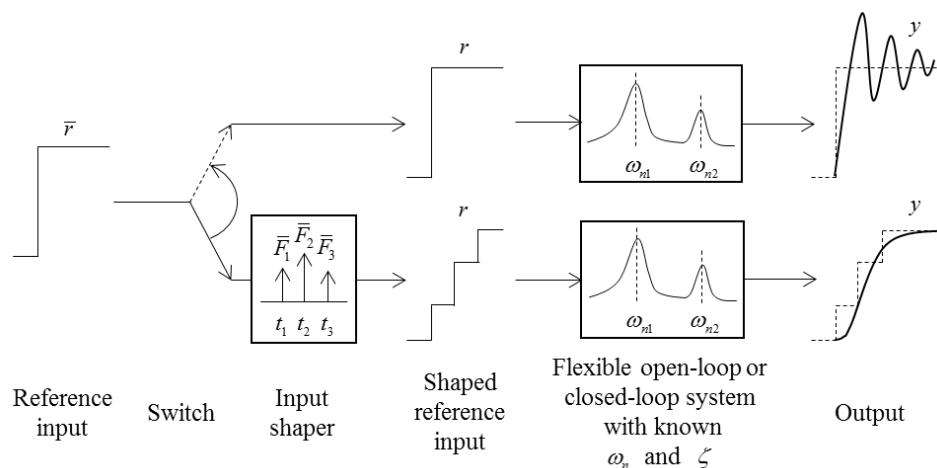


Fig. 1. Input shaping for a flexible system.

Good tutorial documents on the input shaping techniques include Singh and Singhoose in [49], Singhoose in [50], and Singer in [51]. Two text books on input shaping techniques are Singh in [52] and Singhoose and Seering in [53].

In this paper, the proposed system is compared to several types of robust input shapers. For completeness, they are briefly presented in this section with further references given, for more details.

### 2.1.1. ZVD<sup>k</sup> input shaper

Singer and Seering in [7] proposed including higher-order derivatives of the residual vibration expression as additional constraints to provide more robustness to the mode parameter uncertainty at the price of having more impulses in the input shaper sequence and hence slower time to reach final reference value.

ZVD<sup>k</sup> input shaper, where  $k=0, 1, 2, \dots$ , has the total of  $k+2$  impulses in the sequence and is shown to have normalized impulse amplitudes and timings as (Pai in [54]).

$$A_i = \frac{\binom{k+1}{i-1} K^{i-1}}{\sum_{j=0}^{k+1} \binom{k+1}{j} K^j}, \quad t_i = (i-1) \frac{\pi}{\omega_d}, \quad i=1, 2, \dots, k+2, \quad (1)$$

where

$$K = e^{\frac{\zeta\pi}{\sqrt{1-\zeta^2}}}, \quad (2)$$

$$\binom{n}{r} = \frac{n!}{r!(n-r)!} \quad (3)$$

is the combinations of  $n$  things taken  $r$  at a time,  $\zeta$  is the damping ratio,  $\omega_d = \omega_n \sqrt{1-\zeta^2}$  is the damped natural frequency, and  $\omega_n$  is the natural frequency.

### 2.1.2. Extra-insensitive input shaper

Singhoose *et al.* in [38] proposed a one-hump, extra-insensitive (EI) shaper. This shaper has three impulses and a duration equal to that of the ZVD shaper. However, by allowing a low level of vibration  $V_{\text{lim}}$  at the modeling frequency and by forcing the vibration to zero at two frequencies, one lower and the other higher than the modeling frequency, the robustness of the EI shaper is more than that of the ZVD shaper. For undamped system, the normalized impulse amplitudes and timings can be found in closed form as

$$A_1 = \frac{1+V_{\text{lim}}}{4}, \quad t_1 = 0, \quad A_2 = \frac{1-V_{\text{lim}}}{2}, \quad t_2 = \frac{\pi}{\omega_n}, \quad A_3 = \frac{1+V_{\text{lim}}}{4}, \quad t_3 = \frac{2\pi}{\omega_n}. \quad (4)$$

Singhoose *et al.* in [55] extended the one-hump EI shaper to two-hump and three-hump EI shapers, whose number of impulses and duration are the same as the ZVD<sup>2</sup> and ZVD<sup>3</sup>, respectively, but with more robustness. For undamped system, the normalized impulse amplitudes and timings of the two-hump EI shaper can be found exactly as

$$A_1 = \frac{3X^2 + 2X + 3V_{\text{lim}}^2}{16X}, \quad X = \left[ V_{\text{lim}}^2 \left( \sqrt{1-V_{\text{lim}}^2} + 1 \right) \right]^{1/3}, \quad (5)$$

$$A_2 = 0.5 - A_1, \quad A_3 = A_2, \quad A_4 = A_1, \quad (6)$$

$$t_1 = 0, \quad t_2 = 0.5T, \quad t_3 = T, \quad t_4 = 1.5T, \quad (7)$$

where  $T = 2\pi / \omega_n$  is the period of vibration. Those of the three-hump EI shaper are given by

$$A_1 = \frac{1 + 3V_{\text{lim}} + 2\sqrt{2(V_{\text{lim}}^2 + V_{\text{lim}})}}{16}, \quad A_2 = \frac{1-V_{\text{lim}}}{4}, \quad A_3 = 1 - 2(A_1 + A_2), \quad A_4 = A_2, \quad A_5 = A_1, \quad (8)$$

$$t_1 = 0, t_2 = 0.5T, t_3 = T, t_4 = 1.5T, t_5 = 2T. \quad (9)$$

For damped system, the impulse amplitudes and timings cannot be obtained in closed form. They must be solved for numerically. However, a surface fit can be used to obtain their values in terms of  $V_{\text{lim}}$ ,  $\zeta$ , and  $T$ .

### 2.1.3. Impulse-time perturbation input shaper

In the Laplace domain, the ZV input shaper is given by a transfer function

$$F_0(s) = A_1 + A_2 e^{-\tau_d s}, \quad (10)$$

where  $A_1 = 1/(1+K)$ ,  $A_2 = K/(1+K)$ ,  $\tau_d = \pi / (\omega_n \sqrt{1-\zeta^2})$ , and  $K = e^{-\pi\zeta/\sqrt{1-\zeta^2}}$ . Define two perturbed ZV input shapers, for a perturbation parameter  $0 \leq \varepsilon < 1$ , as follows:

$$F_1(s) = A_1 + A_2 e^{-\tau_d(1-\varepsilon)s}, \quad F_2(s) = A_1 + A_2 e^{-\tau_d(1+\varepsilon)s}. \quad (11)$$

A one-hump PEI-IS is given by

$$\begin{aligned} F_{12}(s) &= F_1(s)F_2(s) \\ &= A_1^2 + A_1 A_2 e^{-\tau_d(1-\varepsilon)s} + A_1 A_2 e^{-\tau_d(1+\varepsilon)s} + A_2^2 e^{-2\tau_d s}. \end{aligned} \quad (12)$$

It was shown in Rew *et al.* in [40] that the design parameter  $\varepsilon$  is related to the upper limit of the allowable vibration percentage  $V_{\text{tol}}$  as

$$\varepsilon = \frac{0.9981 \sqrt{V_{\text{tol}}(1-\zeta^2)}}{\pi A_2}. \quad (13)$$

A two-hump PEI-IS is given by

$$F_{012}(s) = F_0(s)F_1(s)F_2(s). \quad (14)$$

A three-hump PEI-IS is given by

$$F_{1234}(s) = F_1(s)F_2(s)F_3(s)F_4(s), \quad (15)$$

where

$$F_3(s) = A_1 + A_2 e^{-\tau_d(1-\delta)s}, \quad F_4(s) = A_1 + A_2 e^{-\tau_d(1+\delta)s}, \quad (16)$$

and  $\delta$  is an additional design parameter.

## 2.2. Intelligent Backstepping Input Shaping

Typical robust input shaping is applied to a closed-loop system as shown in Fig. 2(a), where  $r_b$  is the baseline reference,  $r_s$  is the shaped reference,  $y$  is the plant output,  $u$  is the control effort, and  $e$  is the tracking error. In our flexible-joint robot application,  $\theta_2$  represents the motor shaft's angular position, and  $\theta_1$  is the link's angular position.

The proposed intelligent backstepping input shaping system is shown in Fig. 2(b). The dashed box contains the closed-loop system. By using the states  $x$ , the intelligent backstepping control input  $u_c$  is aimed to reduce the error  $e$  between the plant output  $y$  and the reference model output  $y_m$ . As a result, the closed-loop system, which is a mapping from the shaped reference input  $r_s$  to  $y$  will be close to the known reference model, which is a mapping from  $r_s$  to  $y_m$ . The input shaper then can be designed from mode parameters of the reference model, which are exactly known. Note that the input  $u$  to the plant is the summation of  $u_c$  and  $r_s$ .

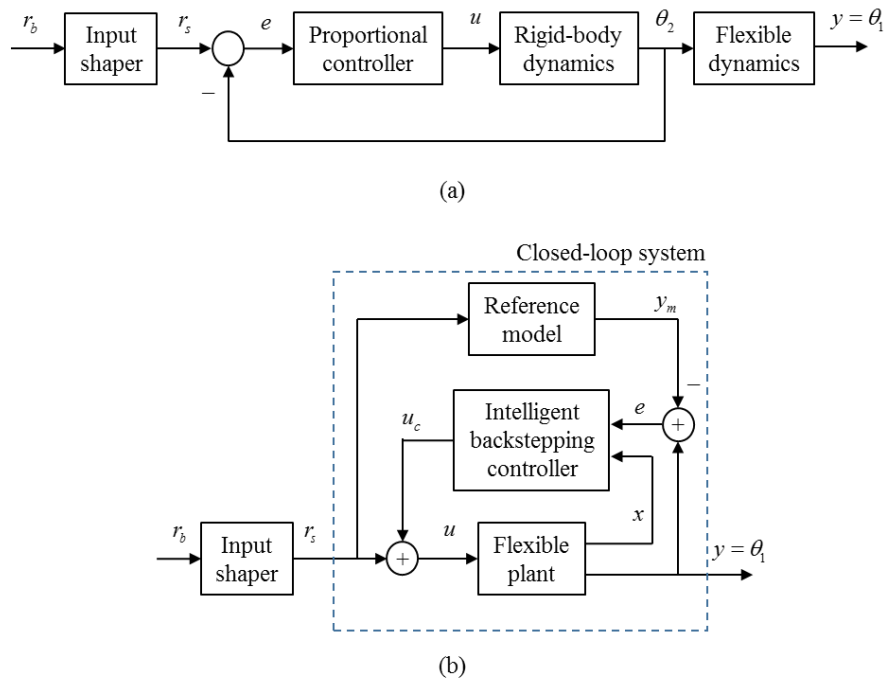


Fig. 2. Input shaping scheme. (a) Typical closed-loop scheme. (b) Proposed closed-loop system.

The flexible plant is assumed to be a single-input-single-output (SISO) system in the strict-feedback form (Krstic *et al.* in [56]) with additive disturbances, that is,

$$\begin{aligned} \dot{x}_i &= f_i(\bar{x}_i) + g_i(\bar{x}_i)(x_{i+1} + d_{ai}(\bar{x}_m)), \quad 1 \leq i \leq m-1, \\ \dot{x}_m &= f_m(\bar{x}_m) + g_m(\bar{x}_m)(u + d_{am}(\bar{x}_m)), \\ y &= x_1, \end{aligned} \tag{17}$$

where  $x_i \in \mathbb{R}$ , are the state variables;  $\bar{x}_i = \{x_1, \dots, x_i\}$ ,  $i = 1, \dots, m$  are the sets of state variables,  $u, y \in \mathbb{R}$  are the control input and plant output,  $f_i(\bullet), g_i(\bullet)$ ,  $i = 1, \dots, m$  are the unknown smooth functions.  $d_{ai}(\bar{x}_m), i = 1, \dots, m$  are the unknown additive disturbances with unknown bounds.

Each unknown smooth function is approximated by a three-layer neural network as shown in Fig. 3. Suppose a scalar-valued continuous function  $g(z_1, z_2, \dots, z_n): \mathbb{R}^n \rightarrow \mathbb{R}$  is to be approximated. The neural network has  $z_1, z_2, \dots, z_n, 1$  as inputs. Variables in the network can be defined as follows:

$$\begin{aligned} \bar{Z} &= [z_1, z_2, \dots, z_n, 1]^T \in \mathbb{R}^{n+1}, \\ V &= [v_1, v_2, \dots, v_l] \in \mathbb{R}^{(n+1) \times l}, \\ v_i &= [v_{i1}, v_{i2}, \dots, v_{i(n+1)}]^T \in \mathbb{R}^{n+1}, \quad i = 1, 2, \dots, l, \\ S(V^T \bar{Z}) &= [s(v_1^T \bar{Z}), s(v_2^T \bar{Z}), \dots, s(v_l^T \bar{Z}), 1]^T \in \mathbb{R}^{l+1}, \\ W &= [w_1, w_2, \dots, w_l, w_{l+1}]^T \in \mathbb{R}^{l+1}, \\ g(W, V, z_1, z_2, \dots, z_n) &= W^T S(V^T \bar{Z}) \in \mathbb{R}. \end{aligned} \tag{18}$$

$s(\bullet)$  can be any appropriate activation function that is a nonconstant, bounded and monotone increasing continuous function (see Theorem 3.1 in Ge *et al.* in [57]). In this work, a sigmoid function  $s(z_i) = 1 / (1 + e^{-z_i}), \forall z_i \in \mathbb{R}$  is used. This network is proved to be a universal approximator in Funahashi in [58], which means any continuous nonlinear function,  $g(z_1, z_2, \dots, z_n)$ , can be approximated by a three-layer neural network with some constant ideal weight matrices,  $W^*, V^*$ , some appropriate number of hidden-layer nodes,  $l$ , with arbitrarily small approximation error.

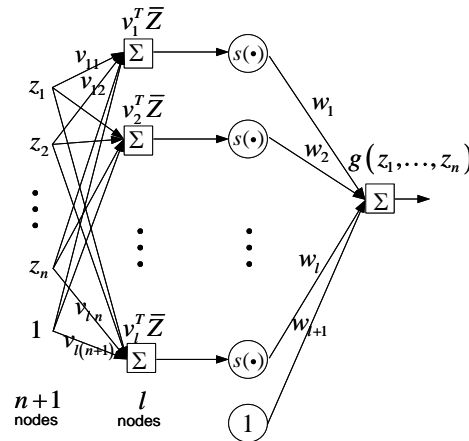


Fig. 3. Three-layer neural network.

For controller design and stability proofs, we need the following assumptions.

**Assumption 1:** Any smooth nonlinear function  $g_i^*(\cdot) \in \mathbb{R}$  can be represented by a three-layer neural network with some constant ideal weights  $W_i^*, V_i^*$  as

$$g_i^*(\cdot) = W_i^{*T} S_i(V_i^{*T} \bar{Z}) + \varepsilon_i \quad (19)$$

where  $\|\varepsilon_i\| < \varepsilon_{iU}$  is the approximation error with unknown  $\varepsilon_{iU} > 0$ ;

**Assumption 2:** On the compact set  $\Omega_z$ , the ideal neural network weights  $W_i^*, V_i^*$  are constant and bounded by

$$\|W_i^*\| \leq W_{iU}, \quad \|V_i^*\|_F \leq V_{iU}, \quad i = 1, \dots, m, \quad (20)$$

where  $W_{iU}$  and  $V_{iU}$  are not known.

**Assumption 3:** Additive disturbances  $d_{ai}(\bar{x}_m, t)$  are bounded by

$$\|d_{ai}(\bar{x}_m, t)\| < d_{aiU}, \quad i = 1, \dots, m, \quad (21)$$

where  $d_{aiU}$  are unknown.

**Assumption 4:** There exist known constants  $g_{iU} > 0$  such that  $\|g_i(\cdot)\| \leq g_{iU} \quad \forall i = 1, \dots, m-1$ .

The lack of knowledge of ideal weights is handled by the following lemma, whose proof can be found in Chapter 3 of Ge *et al.* in [57].

**Lemma 1:** Let  $\hat{W}$  and  $\hat{V}$  be the estimates of  $W^*$  and  $V^*$ , respectively. Let the weight estimation errors be denoted by  $\tilde{W} = \hat{W} - W^*$  and  $\tilde{V} = \hat{V} - V^*$ . Then, we have

$$\hat{W}^T S(\hat{V}^T \bar{Z}) - W^{*T} S(V^{*T} \bar{Z}) = \tilde{W}^T (\hat{S} - \hat{S} \hat{V}^T \bar{Z}) + \hat{W}^T \hat{S} \tilde{V}^T \bar{Z} + d_u, \quad (22)$$

where

$$\begin{aligned} \hat{S} &= S(\hat{V}^T \bar{Z}) \in \mathbb{R}^{l+1}, \\ \hat{S}' &= \text{diag}\{\hat{s}'_1, \hat{s}'_2, \dots, \hat{s}'_l, 0\} \in \mathbb{R}^{(l+1) \times (l+1)}, \\ \hat{s}'_i &= s'(\hat{v}_i^T \bar{Z}) = \left. \frac{d[s(z_a)]}{dz_a} \right|_{z_a = \hat{v}_i^T \bar{z}} \in \mathbb{R}, \quad i = 1, 2, \dots, l, \\ s(z_i) &= 1 / (1 + e^{-z_i}), \quad \forall z_i \in \mathbb{R}. \end{aligned} \quad (23)$$

The residual term  $d_u$  is bounded by

$$|d_u| \leq \|V^*\|_F \|\bar{Z} \hat{W}^T \hat{S}'\|_F + \|W^*\| \|\hat{S}' \hat{V}^T \bar{Z}\| + |W^*|_1. \quad (24)$$

The symbol  $\|\cdot\|_F$  denotes the Frobenius norm.

The control objective is to design an adaptive controller such that the output  $y$  follows closely the reference model output  $y_m$  while all the signals in the closed-loop system are bounded. Backstepping divides control design of the total system in the strict-feedback form (17) into control design of each  $i^{\text{th}}$  subsystem. The control design follows the following steps.

**Step 1:**

Let  $z_1 = x_1 - x_{1d} = y - y_m$  be the model output tracking error. From Assumptions 1-4 and Lemma 1, the following inequality holds:

$$|d_{uf1}| + |\varepsilon_{f1}| + |d_{ug1}x_{2d}| + |\varepsilon_{g1}x_{2d}| + |g_1d_{a1}| \leq K_1^{*T} \varphi_1, \quad (25)$$

where

$$\begin{aligned} K_1^* &= [\|V_{f1}^*\|_F, \|W_{f1}^*\|, \|W_{f1}^*\|_1 + \varepsilon_{f1U} + g_{1U}d_{a1U}, \|V_{g1}^*\|_F, \|W_{g1}^*\|, \|W_{g1}^*\|_1 + \varepsilon_{g1U}]^T, \\ \varphi_1 &= [\|\bar{Z}_{f1}\hat{W}_{f1}^T\hat{S}_{f1}\|_F, \|\hat{S}_{f1}\hat{V}_{f1}^T\bar{Z}_{f1}\|, 1, \|\bar{Z}_{g1}\hat{W}_{g1}^T\hat{S}_{g1}x_{2d}\|_F, \|\hat{S}_{g1}\hat{V}_{g1}^T\bar{Z}_{g1}x_{2d}\|, \|\hat{x}_{2d}\|]^T. \end{aligned} \quad (26)$$

Since  $K_1^*$  is not known, it is estimated by  $\hat{K}_1$  with an estimated error  $\tilde{K}_1 = \hat{K}_1 - K_1^*$ .

Choose a virtual control input

$$\begin{aligned} x_{2d} &= -\hat{g}_1^{-1}[c_1z_1 + \hat{f}_1 - \dot{x}_{1d} - u_{2dvsc}], \\ &= -[\hat{W}_{g1}^T S_{g1}(\hat{V}_{g1}^T \bar{Z}_{g1})]^{-1} [c_1z_1 + \hat{W}_{f1}^T S_{f1}(\hat{V}_{f1}^T \bar{Z}_{f1}) - \dot{x}_{1d} - u_{2dvsc}], \end{aligned} \quad (27)$$

where

$$u_{2dvsc} = -\hat{K}_1^T \varphi_1 \operatorname{sgn}(z_1) \quad (28)$$

is the variable structure controller.

The neural network weights as well as the estimate  $\hat{K}_1$  are updated according to the update laws:

$$\begin{aligned} \dot{\hat{W}}_{f1} &= \dot{\tilde{W}}_{f1} = \Gamma_{wf1}(\hat{S}_{f1} - \hat{S}_{f1}\hat{V}_{f1}^T\bar{Z}_{f1})z_1, \\ \dot{\hat{V}}_{f1} &= \dot{\tilde{V}}_{f1} = \Gamma_{vf1}\bar{Z}_{f1}\hat{W}_{f1}^T\hat{S}_{f1}z_1, \\ \dot{\hat{W}}_{g1} &= \dot{\tilde{W}}_{g1} = \Gamma_{wg1}(\hat{S}_{g1} - \hat{S}_{g1}\hat{V}_{g1}^T\bar{Z}_{g1})x_{2d}z_1, \\ \dot{\hat{V}}_{g1} &= \dot{\tilde{V}}_{g1} = \Gamma_{vg1}\bar{Z}_{g1}\hat{W}_{g1}^T\hat{S}_{g1}x_{2d}z_1, \\ \dot{\hat{K}}_1 &= \dot{\tilde{K}}_1 = \Gamma_{k1}\varphi_1|z_1|, \end{aligned} \quad (29)$$

where  $\Gamma_{wf1}, \Gamma_{vf1}, \Gamma_{wg1}, \Gamma_{vg1}, \Gamma_{k1} > 0$  are design constants.

The tracking error dynamics become

$$\begin{aligned} \dot{z}_1 &= \dot{x}_1 - \dot{x}_{1d} \\ &= f_1 + g_1(x_2 + d_{a1}) - \dot{x}_{1d} + \hat{g}_1x_{2d} - \hat{g}_1x_{2d} + g_1x_{2d} - g_1x_{2d} \\ &= f_1 - \dot{x}_{1d} + \hat{g}_1x_{2d} + g_1d_{a1} + (g_1 - \hat{g}_1)x_{2d} + g_1(x_2 - x_{2d}) \\ &= f_1 - \dot{x}_{1d} + \hat{g}_1[-\hat{g}_1^{-1}[c_1z_1 + \hat{f}_1 - \dot{x}_{1d} + \hat{K}_1^T\varphi_1 \operatorname{sgn}(z_1)]] + g_1d_{a1} + (g_1 - \hat{g}_1)x_{2d} + g_1(x_2 - x_{2d}) \\ &= (f_1 - \hat{f}_1) - c_1z_1 - \hat{K}_1^T\varphi_1 \operatorname{sgn}(z_1) + g_1d_{a1} + (g_1 - \hat{g}_1)x_{2d} + g_1(x_2 - x_{2d}) \\ &= [\varepsilon_{f1} - \tilde{W}_{f1}^T(\hat{S}_{f1} - \hat{S}_{f1}\hat{V}_{f1}^T\bar{Z}_{f1}) - \tilde{W}_{f1}^T\hat{S}_{f1}\tilde{V}_{f1}^T\bar{Z}_{f1} - d_{uf1}] - c_1z_1 - \hat{K}_1^T\varphi_1 \operatorname{sgn}(z_1) + g_1d_{a1} \\ &\quad + [\varepsilon_{g1} - \tilde{W}_{g1}^T(\hat{S}_{g1} - \hat{S}_{g1}\hat{V}_{g1}^T\bar{Z}_{g1}) - \tilde{W}_{g1}^T\hat{S}_{g1}\tilde{V}_{g1}^T\bar{Z}_{g1} - d_{ug1}]x_{2d} + g_1(x_2 - x_{2d}). \end{aligned} \quad (30)$$

Letting a Lyapunov function be

$$V_1 = \frac{1}{2}z_1^2 + \frac{1}{2}\tilde{W}_{f1}^T\Gamma_{wf1}^{-1}\tilde{W}_{f1} + \frac{1}{2}\operatorname{tr}\{\tilde{V}_{f1}^T\Gamma_{vf1}^{-1}\tilde{V}_{f1}\} + \frac{1}{2}\tilde{W}_{g1}^T\Gamma_{wg1}^{-1}\tilde{W}_{g1} + \frac{1}{2}\operatorname{tr}\{\tilde{V}_{g1}^T\Gamma_{vg1}^{-1}\tilde{V}_{g1}\} + \frac{1}{2}\tilde{K}_1^T\Gamma_{k1}^{-1}\tilde{K}_1, \quad (31)$$

its derivative is given by

$$\begin{aligned}
\dot{V}_1 &= z_1 \dot{z}_1 + \tilde{W}_{f1}^T \Gamma_{wf1}^{-1} \dot{\tilde{W}}_{f1} + tr \left\{ \tilde{V}_{f1}^T \Gamma_{vf1}^{-1} \dot{\tilde{V}}_{f1} \right\} + \tilde{W}_{g1}^T \Gamma_{wg1}^{-1} \dot{\tilde{W}}_{g1} + tr \left\{ \tilde{V}_{g1}^T \Gamma_{vg1}^{-1} \dot{\tilde{V}}_{g1} \right\} + \tilde{K}_1^T \Gamma_{k1}^{-1} \dot{\tilde{K}}_1 \\
&= z_1 \left\{ \left[ \varepsilon_{f1} - \tilde{W}_{f1}^T (\hat{S}_{f1} - \hat{S}_{f1}^* \hat{V}_{f1}^T \bar{Z}_{f1}) - \hat{W}_{f1}^T \hat{S}_{f1}^* \tilde{V}_{f1}^T \bar{Z}_{f1} - d_{uf1} \right] - c_1 z_1 - \hat{K}_1^T \varphi_1 \operatorname{sgn}(z_1) + g_1 d_{a1} \right. \\
&\quad \left. + [\varepsilon_{g1} - \tilde{W}_{g1}^T (\hat{S}_{g1} - \hat{S}_{g1}^* \hat{V}_{g1}^T \bar{Z}_{g1}) - \hat{W}_{g1}^T \hat{S}_{g1}^* \tilde{V}_{g1}^T \bar{Z}_{g1} - d_{ug1}] x_{2d} + g_1 (x_2 - x_{2d}) \right\} \\
&\quad + \tilde{W}_{f1}^T \Gamma_{wf1}^{-1} \Gamma_{wf1} (\hat{S}_{f1} - \hat{S}_{f1}^* \hat{V}_{f1}^T \bar{Z}_{f1}) z_1 + tr \left\{ \tilde{V}_{f1}^T \Gamma_{vf1}^{-1} \Gamma_{vf1} \bar{Z}_{f1} \hat{W}_{f1}^T \hat{S}_{f1}^* z_1 \right\} \\
&\quad + \tilde{W}_{g1}^T \Gamma_{wg1}^{-1} \Gamma_{wg1} (\hat{S}_{g1} - \hat{S}_{g1}^* \hat{V}_{g1}^T \bar{Z}_{g1}) x_{2d} z_1 + tr \left\{ \tilde{V}_{g1}^T \Gamma_{vg1}^{-1} \Gamma_{vg1} \bar{Z}_{g1} \hat{W}_{g1}^T \hat{S}_{g1}^* x_{2d} z_1 \right\} + \tilde{K}_1^T \Gamma_{k1}^{-1} \Gamma_{k1} \varphi_1 |z_1| \quad (32) \\
&= z_1 [\varepsilon_{f1} - d_{uf1} - c_1 z_1 - \hat{K}_1^T \varphi_1 \operatorname{sgn}(z_1) + g_1 d_{a1} + \varepsilon_{g1} x_{2d} - d_{ug1} x_{2d} + g_1 z_2] + \tilde{K}_1^T \varphi_1 |z_1| \\
&= z_1 \varepsilon_{f1} - z_1 d_{uf1} - c_1 z_1^2 - \hat{K}_1^T \varphi_1 |z_1| + z_1 g_1 d_{a1} + z_1 \varepsilon_{g1} x_{2d} - z_1 d_{ug1} x_{2d} + z_1 g_1 z_2 + \tilde{K}_1^T \varphi_1 |z_1| \\
&\leq -c_1 z_1^2 + K_1^{*T} \varphi_1 |z_1| - \hat{K}_1^T \varphi_1 |z_1| + z_1 g_{1U} z_2 + \tilde{K}_1^T \varphi_1 |z_1| \\
&= -c_1 z_1^2 + z_1 g_{1U} z_2,
\end{aligned}$$

where  $z_2 = x_2 - x_{2d}$ . The term  $z_1 g_{1U} z_2$  will be cancelled in the next step.

Step i: ( $2 \leq i < m$ )

Let  $z_{i+1} = x_{i+1} - x_{(i+1)d}$ ,  $2 \leq i \leq m-1$ , be the error between the state  $x_i$  and a virtual control law  $x_{id}$ . Similar derivation to that of Step 1 can be used with virtual control input

$$x_{(i+1)d} = -\hat{g}_i^{-1} [g_{(i-1)U} z_{i-1} + c_i z_i + \hat{f}_i - \dot{x}_{id} - u_{(i+1)d\text{vsc}}], \quad 2 \leq i \leq m-1, \quad (33)$$

variable structure control

$$u_{(i+1)d\text{vsc}} = -\hat{K}_i \varphi_i \operatorname{sgn}(z_i), \quad (34)$$

update laws

$$\begin{aligned}
\dot{\hat{W}}_{fi} &= \dot{\tilde{W}}_{fi} = \Gamma_{wfi} (\hat{S}_{fi} - \hat{S}_{fi}^* \hat{V}_{fi}^T \bar{Z}_{fi}) z_i, \\
\dot{\hat{V}}_{fi} &= \dot{\tilde{V}}_{fi} = \Gamma_{vfi} \bar{Z}_{fi} \hat{W}_{fi}^T \hat{S}_{fi}^* z_i, \\
\dot{\hat{W}}_{gi} &= \dot{\tilde{W}}_{gi} = \Gamma_{wgi} (\hat{S}_{gi} - \hat{S}_{gi}^* \hat{V}_{gi}^T \bar{Z}_{gi}) x_{(i+1)d} z_i, \\
\dot{\hat{V}}_{gi} &= \dot{\tilde{V}}_{gi} = \Gamma_{vgt} \bar{Z}_{gi} \hat{W}_{gi}^T \hat{S}_{gi}^* x_{(i+1)d} z_i, \\
\dot{\hat{K}}_i &= \dot{\tilde{K}}_i = \Gamma_{ki} \varphi_i |z_i|.
\end{aligned} \quad (35)$$

and Lyapunov function

$$V_i = V_{i-1} + \frac{1}{2} z_i^2 + \frac{1}{2} \tilde{W}_{fi}^T \Gamma_{wfi}^{-1} \tilde{W}_{fi} + \frac{1}{2} tr \left\{ \tilde{V}_{fi}^T \Gamma_{vfi}^{-1} \tilde{V}_{fi} \right\} + \frac{1}{2} \tilde{W}_{gi}^T \Gamma_{wgi}^{-1} \tilde{W}_{gi} + \frac{1}{2} tr \left\{ \tilde{V}_{gi}^T \Gamma_{vgt}^{-1} \tilde{V}_{gi} \right\} + \frac{1}{2} \tilde{K}_i^T \Gamma_{ki}^{-1} \tilde{K}_i, \quad (36)$$

to obtain the derivative of the Lyapunov function as

$$\dot{V}_i \leq \left( \sum_{k=1}^i -c_k z_k^2 \right) + z_i g_{iU} z_{i+1} \quad (37)$$

Step m:

This is the last step. Let  $z_m = x_m - x_{md}$  be the tracking error. The control effort is selected as

$$u_c = -\hat{g}_m^{-1} [g_{(m-1)U} z_{m-1} + c_m z_m + \hat{f}_m - \dot{x}_{md} - u_{(m+1)d\text{vsc}} + \hat{g}_m r_s]. \quad (38)$$

Note the addition of the last term  $\hat{g}_m r_s$  in the  $u_c$  expression to compensate for the shaped reference  $r_s$ . With similar variable structure control

$$u_{(m+1)dvsc} = -\hat{K}_m \varphi_m \operatorname{sgn}(z_m), \quad (39)$$

update laws

$$\begin{aligned} \dot{\hat{W}}_{fm} &= \dot{\tilde{W}}_{fm} = \Gamma_{vfm} (\hat{S}_{fm} - \hat{S}'_{fm} \hat{V}_{fm}^T \bar{Z}_{fm}) z_m, \\ \dot{\hat{V}}_{fm} &= \dot{\tilde{V}}_{fm} = \Gamma_{vfm} \bar{Z}_{fm} \hat{W}_{fm}^T \hat{S}'_{fm} z_m, \\ \dot{\hat{W}}_{gm} &= \dot{\tilde{W}}_{gm} = \Gamma_{wgm} (\hat{S}_{gm} - \hat{S}'_{gm} \hat{V}_{gm}^T \bar{Z}_{gm}) u z_m, \\ \dot{\hat{V}}_{gm} &= \dot{\tilde{V}}_{gm} = \Gamma_{vgm} \bar{Z}_{gm} \hat{W}_{gm}^T \hat{S}'_{gm} u z_m, \\ \dot{\hat{K}}_m &= \dot{\tilde{K}}_m = \Gamma_{km} \varphi_m |z_m|, \end{aligned} \quad (40)$$

and Lyapunov function

$$\begin{aligned} V_m &= V_{m-1} + \frac{1}{2} z_m^2 + \frac{1}{2} \tilde{W}_{fm}^T \Gamma_{vfm}^{-1} \tilde{W}_{fm} + \frac{1}{2} \operatorname{tr} \{ \tilde{V}_{fm}^T \Gamma_{vfm}^{-1} \tilde{V}_{fm} \} \\ &\quad + \frac{1}{2} \tilde{W}_{gm}^T \Gamma_{wgm}^{-1} \tilde{W}_{gm} + \frac{1}{2} \operatorname{tr} \{ \tilde{V}_{gm}^T \Gamma_{vgm}^{-1} \tilde{V}_{gm} \} + \frac{1}{2} \tilde{K}_m^T \Gamma_{km}^{-1} \tilde{K}_m \\ &= \sum_{k=1}^m \left\{ \frac{1}{2} z_k^2 + \frac{1}{2} \tilde{W}_{fk}^T \Gamma_{vfk}^{-1} \tilde{W}_{fk} + \frac{1}{2} \operatorname{tr} \{ \tilde{V}_{fk}^T \Gamma_{vfk}^{-1} \tilde{V}_{fk} \} \right. \\ &\quad \left. + \frac{1}{2} \tilde{W}_{gk}^T \Gamma_{wgk}^{-1} \tilde{W}_{gk} + \frac{1}{2} \operatorname{tr} \{ \tilde{V}_{gk}^T \Gamma_{vfk}^{-1} \tilde{V}_{gk} \} + \frac{1}{2} \tilde{K}_k^T \Gamma_{kk}^{-1} \tilde{K}_k \right\}, \end{aligned} \quad (41)$$

the derivative of the Lyapunov function becomes

$$\dot{V}_m \leq \left( \sum_{k=1}^m -c_k z_k^2 \right). \quad (42)$$

Therefore, if  $c_k > 0, \forall k = 1, \dots, m$ ,  $\dot{V}_m$  is negative semi-definite or  $\dot{V}_m \leq 0$ . From Theorem 4.1 in Khalil in [59], this results in stable zero equilibrium points of the tracking error dynamics  $\dot{z}_i = \dot{x}_i - \dot{x}_{id}$ , the neural network weight error dynamics  $\dot{\tilde{W}}_{fi}, \dot{\tilde{V}}_{fi}, \dot{\tilde{W}}_{gi}, \dot{\tilde{V}}_{gi}$ , and the variable structure control weight error dynamic  $\dot{\tilde{K}}_i$ .

Several remarks are as follows:

- To avoid chattering due to discontinuous variable structure control laws, the signum  $\operatorname{sgn}(z_i)$  function can be replaced by the smooth  $\arctan(z_i)$  function.
- To prevent the weights  $\hat{W}, \hat{V}$ , and  $\hat{K}$  from growing unboundedly, the  $\sigma$ -modification scheme introduced by Ioannou and Sun in [60] can be applied. In addition, the  $\varepsilon$ -modification by Spooner *et al.* in [61] can be used to prevent the domination of the  $\sigma$  terms leading to poor approximations of the weights.
- Since the control law has a  $\hat{g}_i^{-1}$  term in it, to prevent  $\hat{g}_i$  from approaching zero, which may destabilize the closed-loop system, a discontinuous projection mapping can be applied to confine the weights  $\hat{W}_{gi}$  and hence  $\hat{g}_i$  to values away from zero. For example, assume each element in the weight matrix has desired lower and upper bounds as  $\hat{w}_{i,kLB} \leq \hat{w}_{i,k} \leq \hat{w}_{i,kUB}$ . The projection algorithm is

$$\begin{aligned} \hat{w}_{i,k} &= \operatorname{Proj}_{\hat{w}_{i,k}} \{ \dot{\hat{w}}_{i,k} \} \\ &= \begin{cases} 0 & \text{if } \begin{cases} \hat{w}_{j,k} = \hat{w}_{j,kUB} & \text{and } \dot{\hat{w}}_{i,k} > 0 \\ \hat{w}_{j,k} = \hat{w}_{j,kLB} & \text{and } \dot{\hat{w}}_{i,k} < 0 \end{cases} \\ \dot{\hat{w}}_{i,k} & \text{otherwise.} \end{cases} \end{aligned} \quad (43)$$

The reader is referred to Chatlatanagulchai in [62] and Chatlatanagulchai and Meckl in [63] for selection of design parameters, detailed derivations, and stability proofs.

### 2.3. Flexible-Joint Robot Manipulator

Both simulation and experiment were performed on a flexible-joint robot manipulator, whose photograph is shown in Fig. 4(a). Two optical encoders are used to measure the motor angle  $\theta_2$  and the link angle relative to the motor  $\theta_1 - \theta_2$ . Two soft springs are attached to the link and the motor hub to provide flexibility. Fig. 4(b) contains a top-view diagram of the robot with pertaining dimensions.

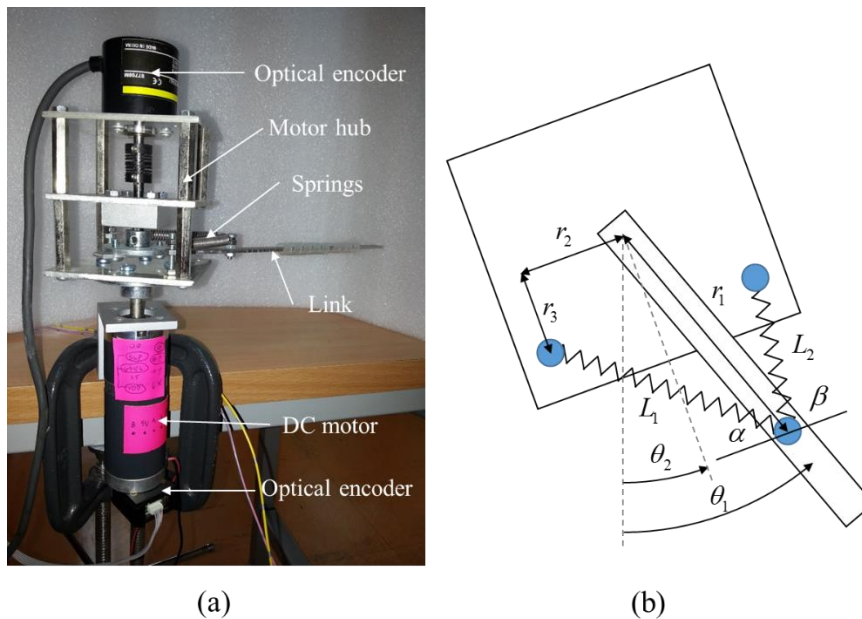


Fig. 4. Flexible-joint robot manipulator: (a) Hardware. (b) Top-view diagram of the robot.

Table 1 contains parameter description and parameter values of the robot, which were obtained from either direct measurements or experimental system identifications. The nonlinear equations of motion of the robot are given in Table 2.  $u$  ( $\pm 2.5$  volts) is the control command voltage from the data acquisition card.  $v$  ( $\pm 24$  volts) is the motor input voltage.  $i$  and  $v$  are the current and voltage in the motor coil.  $T$  is the torque produced by the motor coil.

Table 1. Parameter values of the flexible-joint robot.

Parameter	Description	Values
$l, r_1, r_2, r_3, L$	Link length, dimensions $r_1, r_2, r_3$ in Fig. 4(b), unstretched spring length	0.3 m, 0.1 m, 0.05 m, 0.04 m, 0.02 m
$m_l, m_p$	Link mass, payload mass	0.05 kg, 0.1 kg
$J_l, J_h, J_p$	Link, hub, and payload masses moment of inertia about pivot point	0.0015 kg · m <sup>2</sup> , 0.0011 kg · m <sup>2</sup> , 0.0281 kg · m <sup>2</sup>

$c_1, c_2$	Damping constant at link bearing, damping constant at motor bearing	$0.1 \text{ kg} \cdot \text{s}^{-1}$ , $1 \text{ kg} \cdot \text{s}^{-1}$
$k_s$	Spring constant	$1000 \text{ kg} \cdot \text{s}^{-2}$
$R, L_m, k_v, k_t, k_a$	Motor coil resistance, motor coil inductance, back-EMF constant, current-to-torque gain, amplifier gain	100, 0.01, 0.01, 2000, 9.6

Table 2. Nonlinear governing equations of the flexible-joint robot.

Description	Governing equations
From free-body diagram of the link. $M_k$ is the moment of the nonlinear spring.	$(J_l + J_p)\ddot{\theta}_1 = -c_1(\dot{\theta}_1 - \dot{\theta}_2) + M_k,$ $M_k = -k_s(L_1 - L)(\cos \alpha)r_1 \cos(\theta_1 - \theta_2) + k_s(L_1 - L)(\sin \alpha)r_1 \sin(\theta_1 - \theta_2) + k_s(L_2 - L)(\cos \beta)r_1 \cos(\theta_1 - \theta_2) + k_s(L_2 - L)(\sin \beta)r_1 \sin(\theta_1 - \theta_2),$ $L_1 = \sqrt{(r_1 \cos(\theta_1 - \theta_2) - r_3)^2 + (r_1 \sin(\theta_1 - \theta_2) + r_2)^2},$ $L_2 = \sqrt{(r_1 \cos(\theta_1 - \theta_2) - r_3)^2 + (-r_1 \sin(\theta_1 - \theta_2) + r_2)^2},$ $\alpha = \tan^{-1} \left( \frac{r_1 \cos(\theta_1 - \theta_2) - r_3}{r_1 \sin(\theta_1 - \theta_2) + r_2} \right),$ $\beta = \tan^{-1} \left( \frac{r_1 \cos(\theta_1 - \theta_2) - r_3}{-r_1 \sin(\theta_1 - \theta_2) + r_2} \right)$
From free-body diagram of the motor hub.	$J_h \ddot{\theta}_2 = c_1(\dot{\theta}_1 - \dot{\theta}_2) - M_k - c_2 \dot{\theta}_2 + T$
DC motor electrical model	$v = Ri + L_m \frac{di}{dt} + k_v \dot{\theta}_2,$ $T = k_t i$
Power amplifier	$v = k_a u$

The nonlinear governing equations of the flexible-joint robot in Table 2 can be linearized as

$$\begin{bmatrix} \dot{x}_1 \\ \dot{x}_2 \\ \dot{x}_3 \\ \dot{x}_4 \end{bmatrix} = \begin{bmatrix} 0 & 1 & 0 & 0 \\ -\frac{k_{slin}}{J_l + J_p} & -\frac{c_1}{J_l + J_p} & \frac{k_{slin}}{J_l + J_p} & \frac{c_1}{J_l + J_p} \\ 0 & 0 & 0 & 1 \\ \frac{k_{slin}}{J_h} & \frac{c_1}{J_h} & -\frac{k_{slin}}{J_h} & -\left(\frac{k_t k_v}{J_h R} + \frac{c_2}{J_h} + \frac{c_1}{J_h}\right) \end{bmatrix} \begin{bmatrix} x_1 \\ x_2 \\ x_3 \\ x_4 \end{bmatrix} + \begin{bmatrix} 0 \\ 0 \\ 0 \\ \frac{k_t k_a}{J_h R} \end{bmatrix} T_3, \quad (44)$$

where  $x_1 = \theta_1$ ,  $x_2 = \dot{\theta}_1$ ,  $x_3 = \theta_2$ ,  $x_4 = \dot{\theta}_2$ , and

$$k_{stim} = \left. \frac{\partial M_k}{\partial (\theta_1 - \theta_2)} \right|_{\theta_1 = \theta_2 = 0} = 8.043. \quad (45)$$

Upon substituting the parameter values in Table 1 into (44), the mode parameters, which are the natural frequency and damping ratio, are given by

$$\omega_n = 16.206 \text{ rad/s}, \zeta = 0.052. \quad (46)$$

These natural frequency and damping ratio were used in designing all input shapers in this paper.

### 3. Results and Discussion

The proposed intelligent backstepping input shaping technique in Fig. 2(b) was compared to the typical closed-loop input shaping in Fig. 2(a). In Fig. 2(b), the ZV input shaper was used. In Fig. 2(a), the robust ZVD<sup>k</sup>, EI, and PEI-IS input shapers were used.

In Fig. 2(a), the rigid-body dynamics are from the control effort  $u$  to the motor angular position  $\theta_2$ . The flexible dynamics are from  $\theta_2$  to the link angular position  $\theta_1$ . Both rigid-body and flexible dynamics are the nonlinear governing equations, given in Table 2. The proportional gain was set equal to  $K_p = 0.05$  for all simulation and experiment. The baseline reference signal ( $r_b$ ) was a square wave having an amplitude of 1 radian and a period of 15 seconds. The input shaper is one of the ZVD<sup>k</sup>, EI, and PEI-IS.

In Fig. 2(b), the input shaper is the simple ZV input shaper. The reference model is a second-order underdamped system,

$$\frac{y_m(s)}{r_s(s)} = \frac{\omega_n^2}{s^2 + 2\zeta\omega_n s + \omega_n^2}, \quad (47)$$

where  $\omega_n$  and  $\zeta$  are given by (46). The flexible plant is the nonlinear governing equations in Table 2. The intelligent backstepping controller and update laws are (27)-(40), with the following design parameters:

$$\begin{aligned} c_1 = 1, c_2 = 1, c_3 = 1, c_4 = 50, \\ g_{1U} = 1, g_{2U} = 200, g_{3U} = 1, \\ \Gamma_{ki} = 10, \forall i = 1, \dots, 4, \\ \Gamma_{wf2} = \Gamma_{wf4} = \Gamma_{vf2} = \Gamma_{vf4} = 10, \\ \Gamma_{wg2} = \Gamma_{wg4} = \Gamma_{vg2} = \Gamma_{vg4} = 1. \end{aligned} \quad (48)$$

The number of hidden nodes of all neural networks is five. The inputs to  $\hat{f}_2$  and  $\hat{g}_2$  neural networks are  $x_1$  and  $x_2$ . The inputs to  $\hat{f}_4$  and  $\hat{g}_4$  neural networks are  $x_1, x_2, x_3$ , and  $x_4$ . The initial conditions for the weights are as follows:

$$\begin{aligned} \hat{W}_{f2}(0) = \hat{V}_{f2}(0) = 100, \\ \hat{W}_{f4}(0) = \hat{V}_{f4}(0) = 1, \\ \hat{W}_{g2}(0) = \hat{W}_{g4}(0) = \hat{V}_{g2}(0) = \hat{V}_{g4}(0) = 0.1, \\ \hat{K}_i(0) = 0.1, \forall i = 1, 2, \dots, 4. \end{aligned} \quad (49)$$

Note that  $\hat{f}_1 = \hat{f}_3 = 0$  and  $\hat{g}_1 = \hat{g}_3 = 1$ .

For all simulation and experimental results, the percentage vibration was obtained from the step responses using a formula (Vyhldal *et al.* in [64]):

$$V(\omega_n, \zeta) = \frac{\max(h_{sG}(t)) - h_G(\infty)}{\max(h_G(t)) - h_G(\infty)} \times 100, \quad (50)$$

where  $h_G(t)$  is the step response of the system without the input shaper and  $h_{SG}(t)$  is the step response with the input shaper.

Figure 5 contains two sensitivity curves for the ZV, ZVD, one-hump EI, one-hump PEI-IS, and the proposed intelligent backstepping input shaping (IBS-IS) techniques. Fig. 5(a) is the percentage vibration as a function of the normalized frequency ( $\omega_a / \omega_n$ ), where  $\omega_a$  is the actual natural frequency and  $\omega_n$  is the model natural frequency. Among the robust input shapers, the PEI-IS is the most robust, followed by the EI, ZVD, and ZV shapers. The proposed IBS-IS shaper has literally zero sensitivity to the uncertainty in the natural frequency because the feedback controller matches the uncertain closed-loop system to a fixed reference model. Therefore, the ZV shaper is always designed on the fixed mode parameters. Fig. 5(b) shows the percentage vibration as a function of the damping ratio. Among the robust input shapers, the ZVD has the most robustness, followed by the ZV, PEI-IS, and EI shapers. The proposed IBS-IS shaper also has zero sensitivity to the uncertainty in the damping ratio due to the reasons mentioned above.

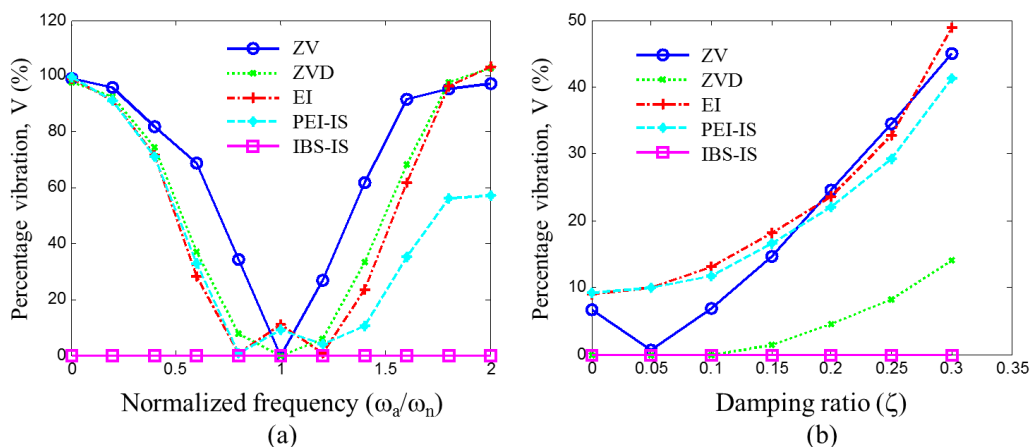


Fig. 5. Sensitivity curves. (a) Percentage vibration as a function of normalized frequency. (b) Percentage vibration as a function of damping ratio.

Figure 6 compares the simulation result to experimental result, using the proposed IBS-IS shaper. The sensitivity curves with respect to the normalized frequency are shown in Fig. 6(a) whereas the sensitivity curves with respect to the damping ratio are shown in Fig. 6(b). The experimental result with the flexible-joint robot is close to the simulation result. Some residual vibration still remains in the experiment because of the unforeseen nonlinearity in the plant.

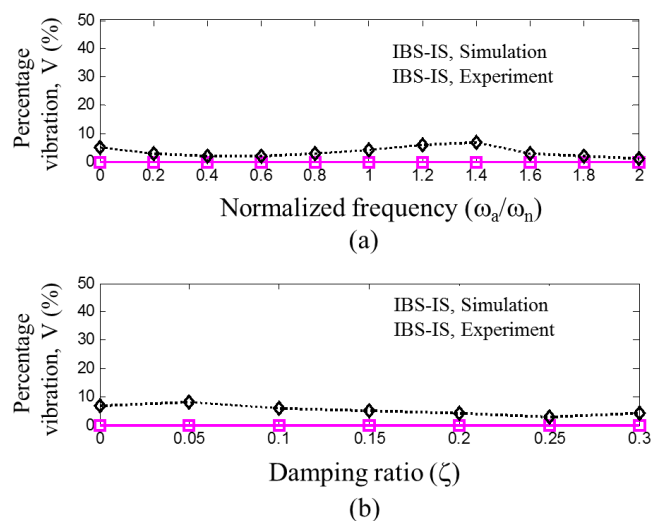


Fig. 6. Simulation and experimental results using the proposed IBS-IS shaper. (a) Sensitivity curve with respect to normalized frequency. (b) Sensitivity curve with respect to damping ratio.

Figure 7 presents input shaper length as a function of 10% insensitivity. The insensitivity is an important measure of robustness in an input shaper. The higher the insensitivity, the more robust the input shaper. Comparing among the robust input shapers, the PEI-IS shaper is the most robust, followed by the EI shaper and the ZVD<sup>k</sup> shaper. The ZVDDD, three-hump EI, and three-hump PEI-IS shapers are the most robust; however, they have the longest shaper length, which affects directly the speed of the robot to reach its final angular position. In the proposed IBS-IS shaper, the shaper length remains at the minimum value, equal to that of the ZV shaper, and the shaper length does not increase with the amount of insensitivity.

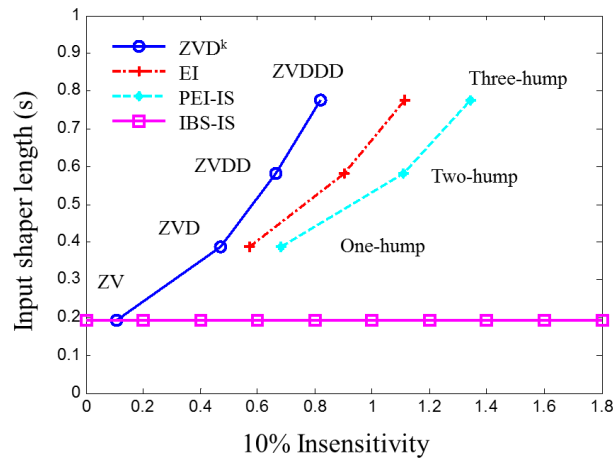


Fig. 7. Input shaper length as a function of insensitivity.

Figure 8 shows simulated link position when payload is time-varying. The payload mass moment of inertia  $J_p$  is increased by 20 percent during the 15<sup>th</sup> to 30<sup>th</sup> seconds and is decreased by 20 percent during the 30<sup>th</sup> to 40<sup>th</sup> seconds. Figure 8(a) contains the result using the ZV shaper whereas Fig. 8(b) contains the result using the proposed IBS-IS shaper. Using the ZV shaper, residual vibration is obvious during the moments when the payload is changed from its model value. Using the proposed IBS-IS shaper, there is literally no residual vibration even during payload variation as a result of the adaptive attribute of the IBS-IS shaper.

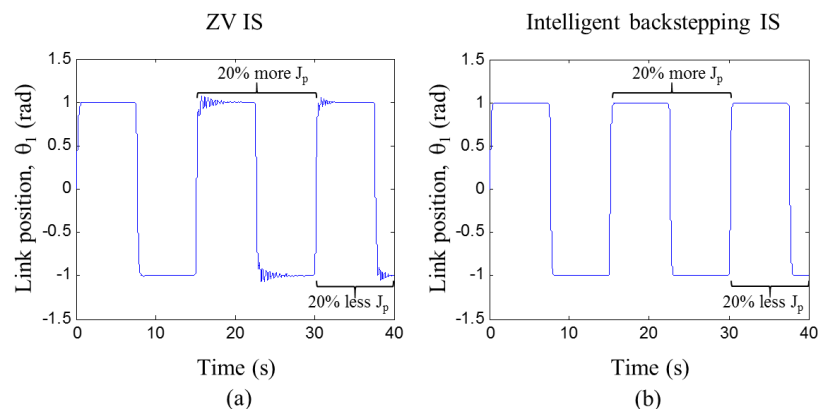


Fig. 8. Simulated link position when payload changes. (a) ZV shaper. (b) Proposed IBS-IS shaper.

Figure 9 contains the percentage vibration as a function of payload deviation percentage. The ZV shaper is the most sensitive to the deviation in payload. The EI and PEI-IS shapers have similar sensitivity because they were both designed to have 10% vibration when the deviation is zero. The ZVD shaper has low level of sensitivity, and the proposed IBS-IS shaper has literally zero sensitivity to payload deviation.

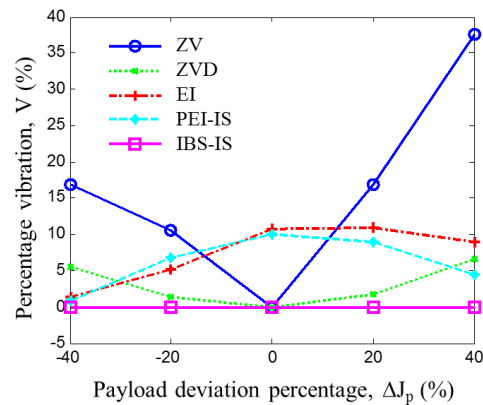


Fig. 9. Percentage vibration as a function of payload deviation percentage.

#### 4. Conclusions

An intelligent backstepping input shaping system is presented. The system uses three-layer neural networks to estimate the unknown plant functions in real time. These estimated plant functions are used in the backstepping and variable structure controllers to match the closed-loop system to a known reference model. The ZV input shaper is placed outside the feedback loop and is designed from the mode parameters of the known and fixed reference model.

From doing so, several benefits include handling of more uncertainty in the plant model, shortest input shaper length, and application to nonlinear and time-varying plant. The use of intelligent system such as three-layer neural networks enables plant model independence, that is, the plant mathematical model is not required in the algorithm. The use of intelligent system in an adaptive setting also enables the proposed system to handle time-varying and configuration-dependent plant.

We have presented in our study:

- The sensitivity curves for the ZV, ZVD, EI, PEI-IS and IBS-IS;
- Simulation and experimental results are done by using the proposed IBS-IS;
- The input shaper length is studied as function of insensitivity (10 % insensitivity);
- The simulated link position for ZV, ZVD, EI, PEI-IS and IBS-IS when payload changes;
- And finally, the percentage vibration for ZV, ZVD, EI, PEI-IS and IBS-IS as function of payload deviation percentage.

#### Acknowledgement

The authors would like to acknowledge the financial support from the master-degree research assistant project, Faculty of Engineering, Kasetsart university, Bangkok, Thailand.

#### References

- [1] O. J. M. Smith, "Posicast control of damped oscillatory systems," *Proc. of the IRE*, vol. 45, no. 9, pp. 1249-1255, Sep. 1957.
- [2] O. J. M. Smith, *Feedback Control Systems*. New York: McGraw-Hill, 1958.
- [3] G. H. Tallman and O. J. M. Smith, "Analog study of dead-beat posicast control," *IRE Trans. on Automatic Control*, vol. 4, no. 1, pp. 14-21, Mar. 1958.
- [4] G. P. Starr, "Swing-free transport of suspended objects with a robot manipulator," in *IEEE Conference on Decision and Control*, San Antonio, TX, 1983, pp. 1484-1487.
- [5] G. P. Starr, "Swing-free transport of suspended objects with a path-controlled robot manipulator," *J. of Dynamic Systems, Measurement, and Control*, vol. 107, no. 1, pp. 97-100, Mar. 1985.
- [6] D. R. Strip, "Swing-free transport of suspended objects: a general treatment," *IEEE Trans. on Robotics and Automation*, vol. 5, no. 2, pp. 234-236, Apr. 1989.
- [7] N. C. Singer and W. C. Seering, "Preshaping command inputs to reduce system vibration," *ASME J. of Dynamics System, Measurement and Control*, vol. 112, no. 1, pp. 76-82, Mar. 1990.

- [8] K. L. Sorensen, W. Singhose, and S. Dickerson, "A controller enabling precise positioning and sway reduction in bridge and gantry cranes," *Control Engineering Practice*, vol. 15, no. 7, pp. 825-837, Jul. 2007.
- [9] K. C. C. Peng, W. Singhose, and D. H. Frakes, "Hand-motion crane control using radio-frequency real-time location systems," *IEEE/ASME Trans. on Mechatronics*, vol. 17, no. 3, pp. 464-471, Jun. 2012.
- [10] J. Huey, H. B. Haraldsson, W. Singhose, J. Lawrence, J. Fortier, S. Wolff, S. K. Sasaki, and E. Watari, "Remote manipulation of cranes via the internet," in *The 8th International Conference on Motion and Vibration Control (MOVIC 2006)*, Daejeon, Korea, 2006, pp. 1-6.
- [11] J. Huang, E. Maleki, and W. Singhose, "Dynamics and swing control of mobile boom cranes subject to wind disturbances," *IET Control Theory and Applications*, vol. 7, no. 9, pp. 1187-1195, Jun. 2013.
- [12] W. Chatlatanagulchai, K. Iemsamai, and J. Soontrajarn, "Vibration reduction in slewing of a very flexible one-link manipulator using shaped reference inputs," *Kasetsart Journal*, vol. 45, no. 6, pp. 1158-1170, Nov. 2011.
- [13] W. Chatlatanagulchai and K. Saeheng, "Real-time reference position shaping to reduce vibration in slewing of a very-flexible-joint robot," *J. of Research in Engineering and Technology*, vol. 6, no. 1, pp. 51-66, Jan. 2009.
- [14] Y. Baozeng and Z. Lemei, "Hybrid control of liquid-filled spacecraft maneuvers by dynamic inversion and input shaping," *ALAA Journal*, vol. 52, no. 3, pp. 618-626, Mar. 2014.
- [15] Y. Zhang and J.-R. Zhang, "Combined control of fast attitude maneuver and stabilization for large complex spacecraft," *Acta Mechanica Sinica*, vol. 29, no. 6, pp. 875-882, Dec. 2013.
- [16] W. E. Singhose, W. P. Seering, and N.C. Singer, "The effect of input shaping on coordinate measuring machine repeatability," in *IFTOMM World Congress on the Theory of Machines and Mechanisms*, Milan, Italy, 1995, pp. 1-5.
- [17] B. Bridgen and W. Singhose, "Comparison of polynomial cam profiles and input shaping for driving flexible systems," *J. of Mechanical Design*, vol. 134, no. 12, pp. 1-7, Nov. 2012.
- [18] J.-Y. Park and P.-H. Chang, "Vibration control of a telescopic handler using time delay control and commandless input shaping technique," *Control Engineering Practice*, vol. 12, no. 6, pp. 769-780, Jun. 2004.
- [19] J. Hongxia, L. Wanli, and W. Singhose, "Using two-mode input shaping to suppress the residual vibration of cherry pickers," in *2011 Third International Conference on Measuring Technology and Mechatronics Automation*, Shangshai, China, 2011, pp. 1091-1094.
- [20] L. Yu and T. N. Chang, "Zero vibration on-off position control of dual solenoid actuator," *IEEE Trans. on Industrial Electronics*, vol. 57, no. 7, pp. 2519-2526, Jul. 2010.
- [21] C. Do, M. Lishchynska, M. Cychowski, K. Delaney, and M. Hill, "Energy-based approach to adaptive pulse shaping for control of RF-MEMS DC-contact switches," *J. of Microelectromechanical Systems*, vol. 21, no. 6, pp. 1382-1391, Dec. 2012.
- [22] C. La-orpacharapan and L. Y. Pao, "Fast seek control for flexible disk drive systems with back EMF and inductance," in *American Control Conference*, Denver, Colorado, 2003, pp. 3077-3082.
- [23] J. Huey and W. Singhose, "Effect of vertical acceleration on the frequency of a pendulum: impact on input shaping," in *IEEE Conference on Control Applications*, Istanbul, Turkey, 2003, pp. 532-537.
- [24] J. Fortgang, V. Patrangenaru, and W. Singhose, "Scheduling of input shaping and transient vibration absorbers for high-rise elevators," in *American Control Conference*, Minneapolis, MN, 2006, pp. 1772-1777.
- [25] T.-S. Yang and W.-L. Liang, "Suppression of nonlinear forced waves by input shaping," *Wave Motion*, vol. 37, no. 2, pp. 101-117, Feb. 2003.
- [26] G. Schitter, P. J. Thurner, and P. K. Hansma, "Design and input-shaping control of a novel scanner for high-speed atomic force microscopy," *Mechatronics*, vol. 18, no. 5, pp. 282-288, Jun. 2008.
- [27] Y. Altintas and M. R. Khoshdarregi, "Contour error control of CNC machine tools with vibration avoidance," *CIRP Annals - Manufacturing Technology*, vol. 61, no. 1, pp. 335-338, Jan. 2012.
- [28] J. Fortgang and W. Singhose, "Concurrent design of vibration absorbers and input shapers," *J. of Dynamic Systems, Measurement, and Control*, vol. 127, no. 3, pp. 329-335, Aug. 2004.
- [29] D. d. Roover and F. B. Sperling, "Point-to-point control of a high accuracy positioning mechanism," in *American Control Conference*, Albuquerque, NM, 1997, pp. 1350-1354.
- [30] H. S. Bae and J. C. Gerdes, "Command modification using input shaping for automated highway systems with heavy trucks," in *American Control Conference*, Denver, CO, 2003, pp. 54-59.
- [31] T. Chang, C. Wang, and E. Cohen, "Speed control of brushless motor using low resolution sensor," in *American Control Conference*, Arlington, VA, 2001, pp. 293-298.

- [32] J. Zhang, R. Lumia, G. Starr, and J. Wood, "Sharing inertia load between multiple robots with active compliant grippers using trajectory pre-shaping," in *IEEE International Conference on Robotics and Automation*, New Orleans, LA, 2004, pp. 2574-2581.
- [33] S. F. Toha and M. O. Tokhi, "Multi-objective PSO based augmented control of a twin rotor system," in *International Conference on Mechatronics*, Kuala Lumpur, Malaysia, 2011, pp. 1-6.
- [34] I. Palunko, R. Fierro, and P. Cruz, "Trajectory generation for swing-free maneuvers of a quadrotor with suspended payload: a dynamic programming approach," in *IEEE International Conference on Robotics and Automation*, Saint Paul, MN, 2012, pp. 2691-2697.
- [35] J. Potter, W. Singhose, and M. Costello, "Reducing swing of model helicopter sling load using input shaping," in *IEEE International Conference on Control and Automation (ICCA)*, Santiago, Chile, 2011, pp. 348-353.
- [36] U. H. Shah and K.-S. Hong, "Input shaping control of a nuclear power plant's fuel transport system," *Nonlinear Dynamics*, vol. 77, no. 4, pp. 1737-1748, Sep. 2014.
- [37] A. Ahmad, M. Z. MdZain, A. R. Abu-Bakar, B. Abd-Ghani, R. Abd-Rahman, and A. As'arry, "Application of input shaping control strategy for reducing chatter noise in the automotive wiper system," in *International Symposium on Information Technology*, Kuala Lumpur, Malaysia, 2008, pp. 1-5.
- [38] W. E. Singhose, W. P. Seering, and N. C. Singer, "Shaping inputs to reduce vibration: a vector diagram approach," in *IEEE International Conference on Robotics and Automation*, Cincinnati, OH, 1990, pp. 922-927.
- [39] N. C. Singer and W. P. Seering, "An extension of command shaping methods for controlling residual vibration using frequency sampling," in *IEEE International Conference on Robotics and Automation*, Nice, France, 1992, pp. 800-805.
- [40] K.-H. Rew, C.-W. Ha, and K.-S. Kim, "An impulse-time perturbation approach for enhancing the robustness of extra-insensitive input shapers," *Automatica*, vol. 49, no. 11, pp. 3425-3431, Nov. 2013.
- [41] T. Singh, "Minimax design of robust controllers for flexible systems," *J. Guid. Control Dyn.*, vol. 25, no. 5, pp. 868-875, Sep. 2002.
- [42] L. Y. Pao, T. N. Chang, and E. Hou, "Input shaper designs for minimizing the expected level of residual vibration in flexible structures," in *American Control Conference*, Albuquerque, NM, 1997, pp. 3542-3546.
- [43] T. Singh, P. Singla, and U. Konda, "Polynomial chaos based design of robust input shapers," *J. of Dynamic Systems, Measurement, and Control*, vol. 132, no. 5, pp. 1-13, Aug. 2010.
- [44] D. P. Magee and W. J. Book, "Implementing modified command filtering to eliminate multiple modes of vibration," in *American Control Conference*, San Francisco, CA, 1993, pp. 2700-2704.
- [45] T. Conord and T. Singh, "Robust input shaper design using linear matrix inequalities," in *International Conference on Control Applications*, Munich, Germany, 2006, pp. 1470-1475.
- [46] J. Vaughan, A. Yano, and W. Singhose, "Performance comparison of robust input shapers," in *IEEE International Conference on Control and Automation*, Guangzhou, China, 2007, pp. 2111-2116.
- [47] J. Vaughan, A. Yano, and W. Singhose, "Performance comparison of robust negative input shapers," in *American Control Conference*, Seattle, WA, 2008, pp. 3257-3262.
- [48] W. Singhose, E. Biediger, Y.-H. Chen, and B. Mills, "Reference command shaping using specified-negative-amplitude input shapers for vibration reduction," *J. of Dynamic Systems, Measurement, and Control*, vol. 126, no. 1, pp. 210-214, Apr. 2004.
- [49] T. Singh and W. Singhose, "Tutorial on input shaping/time delay control of maneuvering flexible structures," in *American Control Conference*, Anchorage, AK, 2002, pp. 1717-1731.
- [50] W. Singhose, "Command shaping for flexible systems: A review of the first 50 years," *Int. J. of Precision Engineering and Manufacturing*, vol. 10, no. 4, pp. 153-168, Oct. 2009.
- [51] N. C. Singer, "Residual vibration reduction in computer controlled machines," Ph.D. dissertation, Department of Mechanical Engineering, Massachusetts Institute of Technology, Cambridge, MA, 1989.
- [52] T. Singh, *Optimal Reference Shaping for Dynamical Systems: Theory and Applications*. Boca Raton: CRC Press, 2010.
- [53] W. Singhose and W. Seering, *Command Generation for Dynamic Systems*, Atlanta: William Singhose, 2011.
- [54] M.-C. Pai, "Robust input shaping control for multi-mode flexible structures using neuro-sliding mode output feedback control," *J. of the Franklin Institute*, vol. 349, no. 3, pp. 1283-1303, Apr. 2012.
- [55] W. E. Singhose, L. J. Porter, T. D. Tuttle, and N. C. Singer, "Vibration reduction using multi-hump input shapers," *J. of Dynamic Systems, Measurement, and Control*, vol. 119, no. 2, pp. 320-326, Jun. 1997.

- [56] M. Krstic, I. Kanellakopoulos, and P. V. Kokotovic, *Nonlinear and Adaptive Control Design*. New York: Wiley, 1995.
- [57] S. S. Ge, C. C. Hang, T. H. Lee, and T. Zhang, *Stable Adaptive Neural Network Control*. New York: Springer, 2002.
- [58] K. I. Funahashi, "On the approximate realization of continuous mappings by neural networks," *Neural Networks*, vol. 2, no. 3, pp. 183-192, May 1989.
- [59] H. K. Khalil, *Nonlinear Systems*, 3rd ed. Upper Saddle River: Prentice Hall, 2002.
- [60] P. A. Ioannou and J. Sun, *Robust Adaptive Control*. Upper Saddle River: Prentice Hall, 1995.
- [61] J. T. Spooner, M. Maggiore, R. Ordonez, and K. M. Passino, *Stable Adaptive Control and Estimation for Nonlinear Systems*. Hoboken: Wiley Interscience, 2002.
- [62] W. Chatlatanagulchai, "Backstepping intelligent control applied to a flexible-joint robot manipulator," Ph.D. dissertation, Department of Mechanical Engineering, Purdue University, West Lafayette, IN, 2006.
- [63] W. Chatlatanagulchai and P. H. Meckl, "Model-independent control of a flexible-joint robot manipulator," *J. of Dynamic Systems, Measurement, and Control*, vol. 131, no. 4, pp. 1-10, Apr. 2009.
- [64] T. Vyhlidal, V. Kucera, and M. Hromcik, "Signal shaper with a distributed delay: Spectral analysis and design," *Automatica*, vol. 49, no. 11, pp. 3484-3489, Nov. 2013.